



# Numerical Study of Winglet Variations on Aerodynamic Performance of NACA 4415 UAV Airfoil

Muhammad Agung Bramantya<sup>1,\*</sup> and Gesang Nugroho<sup>1</sup>

<sup>1</sup> Department of Mechanical and Industrial Engineering, Faculty of Engineering, Universitas Gadjah Mada, Indonesia

Corresponding author's email: [bramantya@ugm.ac.id](mailto:bramantya@ugm.ac.id)

**Abstract.** Technology development and various needs to help humans work without increasing the risk of human safety. One of these technologies is the Unmanned Aerial Vehicle (UAV), commonly referred to as a drone. UAV technology is required in various sectors, both civilian and military. Therefore, research was conducted on the use of winglet variations on the NACA 4415 airfoil to predict aerodynamic performance and to find the best option for winglet geometry on the NACA 4415 airfoil with a wingspan specification of 1100 mm, root chord of 330 mm, and tip chord of 188,5 mm. The research was conducted using the CFD method at a cruising speed of 33,33 m/s and air density of 1,16681 kg/m<sup>3</sup>. There are six variations of winglets in this study: no winglets, fence wingtips, raked wingtips, canted winglets, blended winglets, and split winglets. The results indicate that a wing with a winglet can increase the lift-to-drag ratio (L/D) by approximately 3% to 6% at an angle of attack (AoA) of 0° to 12°. The value of L/D depends on different angles of attack and winglet variations.

**Keywords:** CFD, winglet, NACA 4415, airfoil, aerodynamic performance, UAV

## 1 INTRODUCTION

As technology, especially UAV, continues to advance, it is crucial to fulfill various needs, one of which is surveillance missions. UAV with long-lasting efficiency and durability are necessary for conducting surveillance missions. To achieve this, innovation without altering the shape or reducing the payload of the UAV. One component that can be used to achieve this is the winglet. Winglets can enhance aerodynamic performance (increased coefficient lift and improved L/D ratio) and reduce the occurrence of vortices[5]. Furthermore, changes in the winglet installation angle can influence and enhance aerodynamic performance [3].

Gavrilović conducted research using numerical simulations with a NACA 653218 airfoil. The study included various winglet variations, including no winglets and blended winglets with cant angles of 30°, 45°, 60°, and 90°, performed at different angles of attack (AoAs) of 0°, 2°, 4°, 6°, 8°, 10°, 12°, and 14°. The study was conducted under a pressure of 101325 Pa pressure, 288,2 K air temperature, and speed of Mach 0,2. The tip chord length of the airfoil was 1,775 m, and the root chord length was 4,17 m. The results revealed that the optimal and suitable winglet for the given airfoil type, 30°, cant angle of 45°, cant angle of 90°, and no winglet [4] based on the lift-to-drag ratio, was a blended winglet with a cant angle of 60°. The winglet results, based on the highest to lowest L/D ratios, were as follows: blended winglet with a cant angle of 60°,

cant angle of  $30^\circ$ , cant angle of  $45^\circ$ , cant angle of  $90^\circ$ , and no winglet [4]. In this paper there are six variations winglet were used, No winglet, Fence wingtip, Canted winglet, Raked wingtip, Blended winglet, and Split winglet.

## 2 METHODOLOGY

In this study, numerical simulations were performed using ANSYS software. The semi-implicit pressure-linked equations (SIMPLE) method was employed. This method was well suited for this study because the operating conditions were steady, incompressible, and capable of capturing flow separation. The accuracy of the numerical simulation results depends significantly on the choice of method. To obtain accurate results, it is essential to select an appropriate method that aligns with a desired approach.

### 2.1 Geometric Model Design

Table 1 presents the geometric specifications of the wing configuration without winglets. The other winglet variations had the same specifications, except for the wing area.

**Table 1.** Specification geometry of the wing

Parameters	Values
Chord Tip	188,5 mm
Chord Root	330 mm
Wing Area	0,275 m <sup>2</sup>
Wingspan	1100 mm

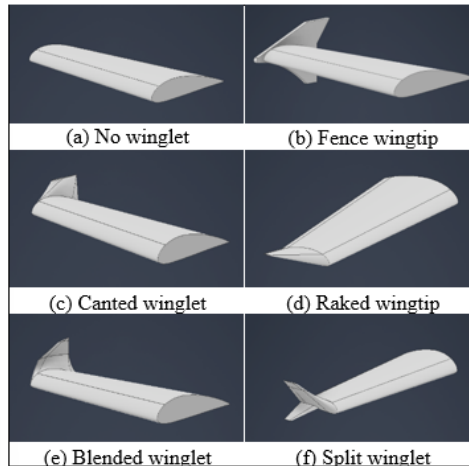


**Fig. 1.** Design of the winglet variations

Figure 1 shows the design of the wing geometry with winglet variation. Six variations were used to study the effects of winglet geometry on UAV performance.

### 2.2 Mesh Generation

In this study, a polyhedral mesh was used for meshing. Body sizing and face sizing were applied to all winglet geometries to improve the mesh quality. Additionally, inflation was used around the airfoil surface to capture and refine the airflow passing through. Figure 2 shows the fluid domains used in this study. The results of the meshing performed on all winglet variations were below 0.25 (skewness quality). According to ANSYS, the meshing performance was excellent. The size of the fluid domain in this study was five times the length of the root chord of the airfoil for the front, top, and bottom sections and 15 times the length of the root chord of the airfoil for the rear section.

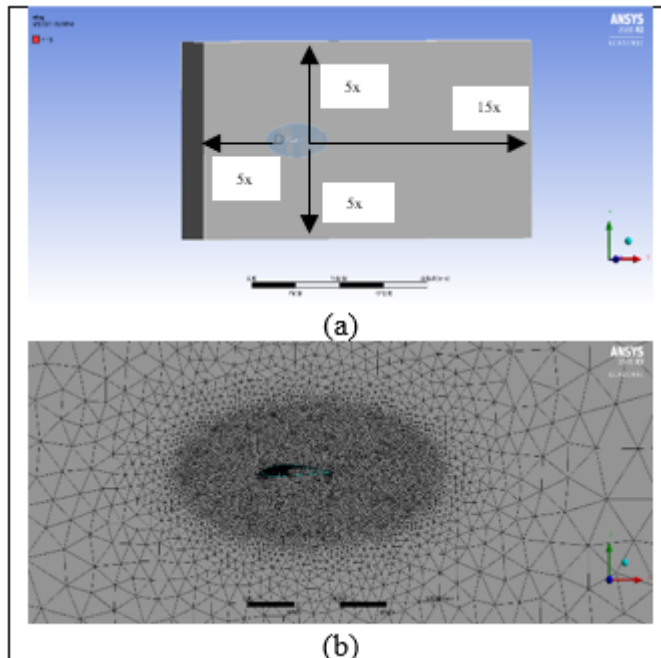


Fig. 2. (a) Fluid domain (b) Mesh visualization.

### 2.3 Governing Equation

The governing equation, also known as the governing equation or governing equation, is the main equation that models a form of fluid flow. According to Anderson, the governing equation can be divided into three core equations: the continuity equation or law of conservation of mass, the law of conservation of energy, and the law of conservation of momentum. These three equations are expressed as follows.

1. Continuity Equation:

$$\frac{\partial \rho}{\partial t} + \nabla \cdot (\rho v) = 0 \text{ atau } \frac{\partial \rho}{\partial t} + \frac{\partial \rho u}{\partial x} + \frac{\partial \rho v}{\partial y} + \frac{\partial \rho w}{\partial z} = 0 \tag{1}$$

## 2. Energy-conservation equation

$$\begin{aligned}
 \frac{\partial E_T}{\partial t} + \frac{\partial(uE_T)}{\partial x} + \frac{\partial(vE_T)}{\partial y} + \frac{\partial(wE_T)}{\partial z} \\
 = -\frac{\partial(uP)}{\partial x} - \frac{\partial(vP)}{\partial y} - \frac{\partial(wP)}{\partial z} - \frac{\mu}{Pr} \left( \frac{\partial q_x}{\partial x} + \frac{\partial q_y}{\partial y} + \frac{\partial q_z}{\partial z} \right) \\
 + \mu \left[ \frac{\partial}{\partial x} (u\tau_{xx} + v\tau_{yz} + z\tau_{zz}) + \frac{\partial}{\partial y} (u\tau_{xy} + v\tau_{yy} + z\tau_{yz}) \right. \\
 \left. + \frac{\partial}{\partial z} (u\tau_{xz} + v\tau_{yz} + z\tau_{zz}) \right]
 \end{aligned} \tag{2}$$

## 3. Momentum Conservation Equation:

For the x-direction of flow,

$$\frac{\partial(\rho u)}{\partial t} + \frac{\partial(\rho u^2)}{\partial x} + \frac{\partial(\rho uv)}{\partial y} + \frac{\partial(\rho uw)}{\partial z} = -\frac{\partial P}{\partial x} + \rho g_x + \mu \left( \frac{\partial \tau_{xx}}{\partial x} + \frac{\partial \tau_{xy}}{\partial y} + \frac{\partial \tau_{xz}}{\partial z} \right) \tag{3}$$

For the y-direction of flow,

$$\frac{\partial(\rho v)}{\partial t} + \frac{\partial(\rho uv)}{\partial x} + \frac{\partial(\rho v^2)}{\partial y} + \frac{\partial(\rho vw)}{\partial z} = -\frac{\partial P}{\partial y} + \rho g_y + \mu \left( \frac{\partial \tau_{xy}}{\partial x} + \frac{\partial \tau_{yy}}{\partial y} + \frac{\partial \tau_{yz}}{\partial z} \right) \tag{4}$$

For the z-direction of the flow,

$$\frac{\partial(\rho w)}{\partial t} + \frac{\partial(\rho uw)}{\partial x} + \frac{\partial(\rho w^2)}{\partial z} + \frac{\partial(\rho vw)}{\partial y} = -\frac{\partial P}{\partial z} + \rho g_z + \mu \left( \frac{\partial \tau_{xz}}{\partial x} + \frac{\partial \tau_{yz}}{\partial y} + \frac{\partial \tau_{zz}}{\partial z} \right) \tag{5}$$

## 2.4 Boundary Condition

The boundary condition was illustrated in Figure 3. The inlet velocity was defined 33,33 m/s, and the outlet was set as the pressure outlet. The UAV operates at a low altitude (150 m) above the sea level. The wing surface was assumed to have no slippage.

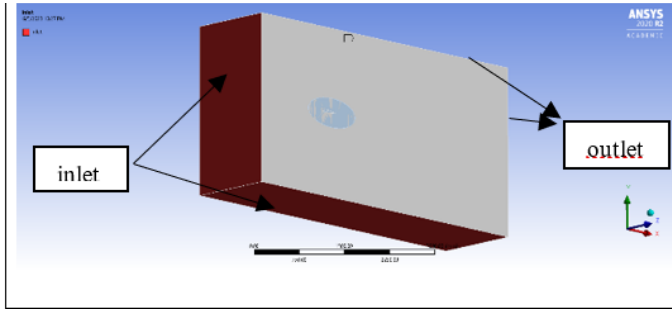


Fig. 3. Boundary Condition

### 2.5 Grid Dependency Check

To initiate a CFD simulation, it is crucial to explore the impact of mesh size on the accuracy of the solution outcomes. Typically, increasing the number of cells enhances the numerical accuracy. However, this also entails higher demand for computer memory and computational time. It should be noted that changing the cell number does not affect the lift results. To assess the independence of the results from cell counts, five distinct mesh sizes were generated. The results are presented in Table 2.

Table 2. Comparison of meshes with different cell numbers

Cell Number	196292	24030	30236	388373	51764
	3	74	00	9	08
Lift	24,17	25,24	25,38	25,23	25,12

As shown in Table 2, the selection of the cell number ranges was approximately 3023600 cells. The results show that at a particular cell number, the resulting lift is also better than that of other cell numbers. In addition, the quality of the generated mesh also meets the criteria and refers to ANSYS parameter with a skewness quality below 0,25 (excellent) and an orthogonal quality above 0,75 (very good).

## 3 RESULT AND DISCUSSION

Based on the results of the numerical simulation conducted in this study, it was found that each variation in the winglet affected the aerodynamic performance. The lift force in this study is represented by the coefficient of lift (CL) value. For the lift coefficient value, the stall angle and CL max of each winglet variation were observed. Figure 4 shows a graph representing CL versus AoA for all winglet variations. From the data and graph, we can see that there was an increase in the CL value from 0° to 12° AoA for each winglet variation. After surpassing 12° AoA, a decrease in the CL value and the occurrence of the stall phenomenon were observed in all winglet variations. A stall occurs when flow separation occurs on the aircraft wing surface, leading to a decrease in the velocity on the upper wing surface. At 12° AoA, each winglet variation achieves

its maximum CL value. The maximum CL values for each winglet, from highest to lowest, were raked, canted, split, blended, and fence.

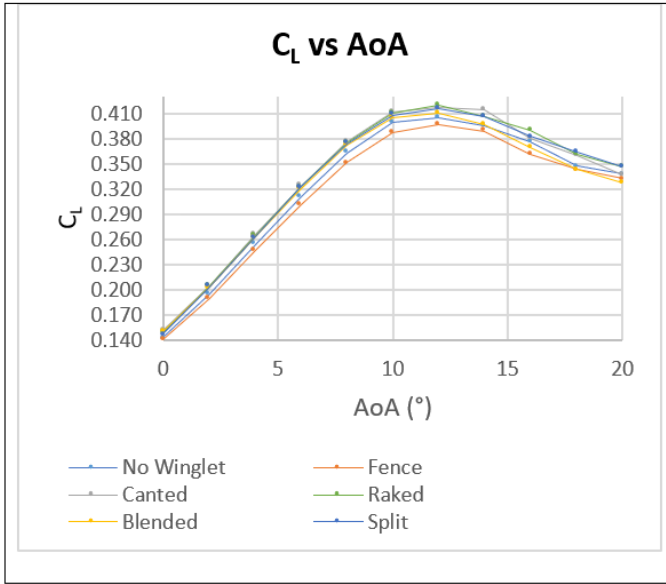
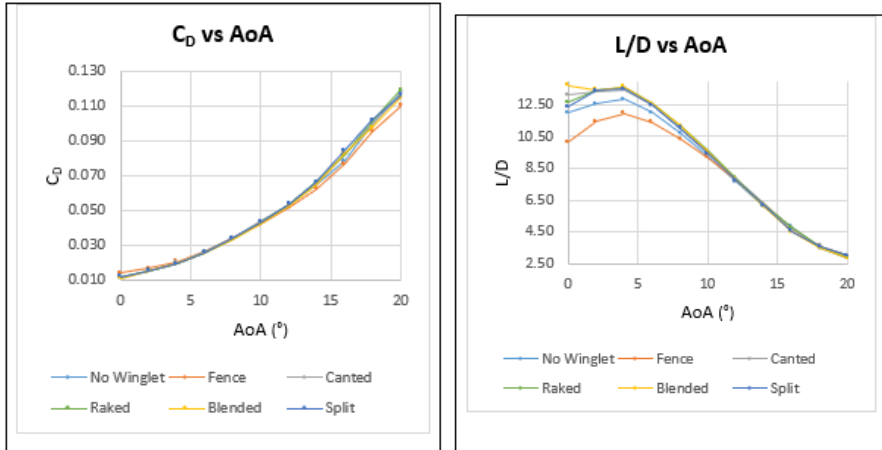


Fig. 4. Graph CL vs AoA

The addition of winglets resulted in a greater lift force compared to the case without winglets. At 0° AoA, the winglet variations that produce higher CL values compared to the no winglet variation are canted with 5.97%, blended with 5.29%, raked with 4.12%, and split with 3.19%, respectively. These variations generated a larger lift force than the no-winglet variation did. However, the fence variation produces a 1.54% lower lift force than the no-winglet variation. In the study conducted by Gongzhang and Axtelius (2020), it can be concluded that the addition of winglet geometry should increase the lift force and CL. However, in this study, the CL value for the no-winglet variation was greater than that for the fence variation at all the AoA values. This was because the fence variation had a significantly larger winglet area, causing the CL value for the no-winglet variation to be greater when calculated. If the increase in the winglet area is not excessively large, then the CL value for the fence variation would be greater than the CL value for the no-winglet variation at all AoAs.



**Fig. 5. (a) Graph  $C_L$  vs AoA, (b) Graph L/D vs AoA**

In figure 5(a), the processed data from the numerical simulation are presented in the form of graphs. From the data, it can be observed that  $C_D$  increased with increasing AoA for each winglet variation. The results of the winglet variations show that the  $C_D$  values at the highest AoA, which is  $20^\circ$ , ranked from highest to lowest, are raked, no winglet, canted, split, blended, and fenced. The higher the  $C_D$  value, the greater the resulting drag force; conversely, the lower the  $C_D$  value, the lower the drag force generated. Ideally, in this study, it was desirable to achieve a low drag force. Next, at AoA  $12^\circ$ , where the  $C_L$  max occurs, the  $C_D$  values from highest to lowest are split, canted, raked, no winglet, blended, and fence. Overall, it can be concluded that the addition of winglet geometry increases the drag from AoA  $0^\circ$  to AoA  $12^\circ$ . However, after an AoA greater than  $12^\circ$ , the addition of winglet geometry reduced the drag force. This implies that the addition of the winglet geometry can reduce the drag under stall conditions.

The L/D ratio (L/D) is an indicator that helps to determine the aerodynamic performance and efficiency of an airfoil. A higher lift-to-drag ratio indicates a better airfoil performance and efficiency, whereas a lower lift-to-drag ratio indicates a poorer performance and efficiency. The lift-to-drag ratio is calculated by dividing the lift force by the drag force.

In figure 5(b), it can be seen that the blended variation yields a better L/D ratio than the other variations. However, from  $14^\circ$  to  $20^\circ$  AoA, the raked variation performed better. In other words, after the occurrence of stall at an AoA of  $12^\circ$ , the raked variation was superior to the blended variation owing to its higher L/D ratio. When considering the L/D values across all AoAs, the variations rank from highest to lowest L/D ratio as follows: blended, canted, raked, split, no winglet, and fence. At an AoA of  $4^\circ$ , as shown in figure 6, the highest L/D ratio was observed for all winglet variations. However, after surpassing AoA  $4^\circ$ , the L/D ratio started to decrease for all winglet variations. This is consistent with the velocity contours and pressure contours of the mid-wing cross-section for all winglet variations.

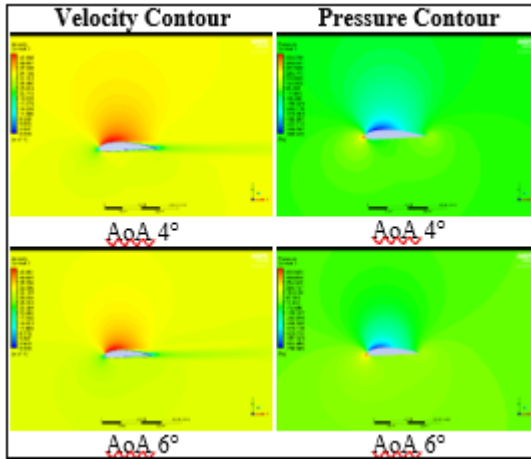


**Fig. 6.** Velocity and pressure contours for fence variation

In Figure 6, an example of the pressure contours and velocity contours at AoA  $4^\circ$  for fence variation can be observed. It can be seen that there is an initial onset of flow separation in the trailing edge area of the airfoil. As AoA increased, the flow separation became more pronounced and evident. At AoA  $0^\circ$ , the L/D values from highest to lowest are as follows: blended with 14.55%, canted with 9.39%, raked with 5.69%, and split with 3.26%, all of which are greater than the no winglet variation. However, the fence variation decreased by 15.29% owing to an excessively large winglet area. At AoA  $12^\circ$ , where CL max occurs, the L/D values from highest to lowest are as follows, raked 3.24%, canted with 2.38%; blended with 2.22%; split with 1.59%; and fence 1.47%, all of which are higher than the no-winglet variation. The highest L/D value was achieved by the blended variation at AoA  $0^\circ$  with a value of 13,74.

On average, if the wing operates at the optimal AoA range from  $0^\circ$  to  $12^\circ$  (CL max), the L/D performance can improve by up to 5.99% using the blended geometry variation compared with the no-winglet variation. Furthermore, on average L/D performance across all AoA, the wing can improve by up to 3.35% using the raked variation compared to the no winglet variation.

## 4 CONCLUSION

Based on the simulations conducted on the NACA 4415 airfoil with various winglet geometries, including no winglets, fence wingtips, canted wingtips, raked wingtips, blended winglets, and split winglets, at angles of attack (AoA) of  $0^\circ$ ,  $2^\circ$ ,  $4^\circ$ ,  $6^\circ$ ,  $8^\circ$ ,  $10^\circ$ ,  $12^\circ$ ,  $14^\circ$ ,  $16^\circ$ ,  $18^\circ$ , and  $20^\circ$ , several conclusions can be drawn to answer some questions related to the research problem and objectives.

The aerodynamic performance of the wings was assessed based on their L/D ratio. Among all the winglet variations, the blended winglet at AoA  $0^\circ$  provides the highest improvement in aerodynamic performance, with an increase of up to 14.55% compared to the no-winglet variation. Furthermore, at AoA  $12^\circ$ , where CL max occurs, the raked wingtip variation shows the highest improvement in wing performance, with an

increase of up to 3.24% compared to the no-winglet variation. On average, when the wing was operated under all AoA conditions, the aerodynamic performance improved by 3.35%.

There are two options for suitable winglet geometry variations for the NACA 4415 airfoil, based on the L/D ratio. Considering the average wing performance across all AoAs, the use of raked wingtip variation was the best choice for the NACA 4415 airfoil. In the second option, if the wing operates in the optimal range of AoA from 0° to 12°, the use of the blended winglet geometry variation provides the best choice for the NACA 4415 airfoil.

## REFERENCES

1. (2017). ANSYS Fluent Users Guide, SAS IP, Inc
2. Clancy, L. J. (1975). Aerodynamics. Pitman Publishing Limited
3. Tjahjana, D.D.D.P.; Yaningsih, I.; Imama, B.Y.L.; and Prabowo, A.R. (2021). EVERGREEN Joint Journal of Novel Carbon Resource Sciences & Green Asia Strategy, 8(4), 799–811
4. Gavrilović, N.N.; Rašuo, B.P.; Dulikravich, G. S.; Parezanović, V. (2014). Faculty of Mechanical Engineering, Belgrade
5. Gongzhang, H.; and Axtelius, E. (2020). Degree Project in Vehicle Engineering, Second Cycle, 15 Credits Stockholm, Sweden
6. Güzelbey, I.H.; Eraslan, Y.; and Dođru, M. H. (2019). European Mechanical Science. Turkey, 3(1), 18–23
7. Helal, H.S.M.; Khalil, E.K.E.; Abdellatif, O.A.E.; and Elhariry, G.E.M. (2016). IOSR Journal of Mechanical and Civil Engineering, 13(3), 65–72
8. Panagiotou, P.; Kaparos, P.; and Yakinthos, K. (2014). Aerospace Science and Technology, 39, 190–205
9. Raymer, D. P. (1992). American Institute of Aeronautics and Astronautics, Inc.
10. Reddy, S. R., Sobieczky, H., Dulikravich, G. S., & Abdoli, A. (2016). Journal of Aircraft, 53(4), 992–1000
11. Roskam, J. (1985). Design, Analysis and Research Corporation (Darcorporation)
12. Roy, S. (2018). International Journal of Mechanical Engineering (IJME), 7(2)
13. Rubel, R. I.; Uddin, M. K.; Islam, M. Z.; and Rokunuzzaman, M. (2016). International Journal of Research – GRANTHAALAYAH, 5(11), 187-197
14. Versteeg, H. K.; and Malalasekera, W. (1995). Pearson Education Limited
15. Wibowo, S. B.; Sutrisno, and Rohmat, T.A. (2019). International Journal of Fluid Mechanics Research, 46(5), 427–439
16. Öztürk, Ş.; and Örs, İ. (2020). International Journal of Aeronautics and Astronautics, 1(1), 1–11

**Open Access** This chapter is licensed under the terms of the Creative Commons Attribution-NonCommercial 4.0 International License (<http://creativecommons.org/licenses/by-nc/4.0/>), which permits any noncommercial use, sharing, adaptation, distribution and reproduction in any medium or format, as long as you give appropriate credit to the original author(s) and the source, provide a link to the Creative Commons license and indicate if changes were made.

The images or other third party material in this chapter are included in the chapter's Creative Commons license, unless indicated otherwise in a credit line to the material. If material is not included in the chapter's Creative Commons license and your intended use is not permitted by statutory regulation or exceeds the permitted use, you will need to obtain permission directly from the copyright holder.

